Viscous normal stresses and fingertip tripling in radial Hele-Shaw flows

Írio M. Coutinho,[1,*] Francisco M. Rocha [2,†] and José A. Miranda [1,‡]

[1]*Departamento de Física, Universidade Federal de Pernambuco, Recife, Pernambuco 50670-901, Brazil*
[2]*Aix Marseille University, CNRS, IUSTI, 13453 Marseille, France*

Viscous fingering in radial Hele-Shaw cells is markedly characterized by the occurrence of fingertip splitting, where growing fingered structures bifurcate at their tips, via a tip-doubling process. A much less studied pattern-forming phenomenon, which is also detected in experiments, is the development of fingertip tripling, where a finger divides into three. We investigate the problem theoretically, and employ a third-order perturbative mode-coupling scheme seeking to detect the onset of tip-tripling instabilities. Contrary to most existing theoretical studies of the viscous fingering instability, our theoretical description accounts for the effects of viscous normal stresses at the fluid-fluid interface. We show that accounting for such stresses allows one to capture the emergence of tip-tripling events at weakly nonlinear stages of the flow. Sensitivity of fingertip-tripling events to changes in the capillary number and in the viscosity contrast is also examined.

I. INTRODUCTION

When a lower viscosity fluid is injected against a higher viscosity one in the narrow gap between the parallel glass plates of a radial Hele-Shaw cell, the initially circular interface separating them becomes unstable and deforms. During this deformation process, the interface develops protrusions that resemble the shape of fingers [1]. As the penetrating fingers grow, they widen, and get increasingly flat at their extremities. Then, the flattened fingers split at their tips, mostly dividing into two new, smaller fingers. Such a typical tip-splitting phenomenon in which a growing finger branches out into two smaller fingers characterizes a pattern-forming behavior that can be more precisely defined as tip doubling. The succession of fingertip-doubling events increases the complexity of the expanding fluid-fluid interface, leading to the formation of highly branched structures at advanced time stages of the evolution [2–7]. The tip-doubling phenomenon is the most emblematic pattern-forming process in radial Hele-Shaw flows. These convoluted fluid dynamic shapes arise due to the Saffman-Taylor instability [8], and are commonly referred to as viscous fingering patterns.

Irrespective of the large number of investigations of the injection-driven radial viscous fingering problem performed during the past few decades, the vast majority of these studies neglect the effects of viscous normal stresses [9] on the dynamics of the fingered structures. As a matter of fact, in the context of Hele-Shaw flows, just a few theoretical research groups have analyzed the impact of viscous normal stresses on the evolving fluid-fluid interface. For example, in Ref. [10] a linear stability analysis has shown that the inclusion of

normal stress effects leads to a more accurate prediction for the number of resulting fingers that are formed in the centrifugally driven viscous fingering problem in rotating Hele-Shaw cells. By taking into account the presence of viscous normal stresses, the authors of Ref. [10] have derived a linear dispersion relation for the rotating problem, and from it obtained an analytical prediction for the number of emerging fingers. It turns out that this theoretical prediction was in an increased agreement with their experimental measurements than the corresponding prognosis which neglects normal viscous stresses. Later, now in the context of the injection-driven situation in radial Hele-Shaw cells, Kim *et al.* [11] executed a linear stability analysis of the problem, and showed that normal stresses change the speed of propagation of the undisturbed interface, and also modify the linear growth rate, consequently altering the value of the mode of maximum growth, a popular linear predictor for the number of fingers that arise at the interface during initial linear stages of the flow. In Ref. [11] it has been demonstrated that the addition of the viscous normal stresses stabilizes the system, and brings their linear theory into a better agreement with experiments in radial Hele-Shaw cells driven by injection.

After the seminal work by Kim *et al.* [11] some other groups investigated the effects of viscous normal and other stresses on viscous fingering in Hele-Shaw cells at the linear level. For instance, Awasthi *et al.* [12] utilized Darcy's law, and included the effects of shearing (tangential) stresses in the viscous potential flow analysis of radial fingering in a Hele-Shaw cell, showing that such stresses further stabilize the system. Nagel and Gallaire [13] used the Brinkman equation and took into account both normal and tangential viscous stresses to derive a quite complicated linear dispersion relation for the Saffman-Taylor instability, finding a good accordance with experiments. The consideration of interfacial fingering and normal viscous stresses effects has also been instrumental to provide a better agreement between theoretical predictions

*iriomenezes@gmail.com
†francisco.rocha@univ-amu.fr
‡jose.mirandant@ufpe.br

and experiments for fluid adhesion problems in Hele-Shaw geometry [14].

In addition to the stability analyses which considered the role of viscous normal stresses only at the purely linear stages of the flow [10–14], there are a few studies that examined the impact of such stresses in the early nonlinear regime of the pattern-forming dynamics. Linear theory provides useful information about the stability of the interface, and the typical number of arising fingers. On the other hand, nonlinear perturbative mode-coupling theory allows one to predict and capture key elements related to the morphology of the patterns [15–19]. In this way, one can investigate how the shape of the fingers is affected by the inclusion of normal stresses at the onset of nonlinearities. Second-order weakly nonlinear studies considering the presence of viscous normal stresses have been performed in Refs. [20,21]. Reference [20] reinforced the necessity of introducing normal stresses into the general theoretical framework of the rotating Hele-Shaw cell problem in order to obtain a better and more reliable understanding of the nonlinear finger competition dynamics observed in experiments. Moreover, in Ref. [21] it has been found that the introduction of normal stresses does affect the iconic tip-doubling phenomenon that occurs in radial Hele-Shaw flows induced by injection. The second-order study implemented in Ref. [21] has indicated that, even though the maximal growth rate is decreased by the action of normal stress at the linear level [11], at the beginning of nonlinear stages it leads to further development of characteristic finger bifurcation events in which a single finger divides into two.

Despite the large number of works on radial viscous fingering which neglect the action of viscous normal stresses, and the considerably smaller number of studies which take them into account, one feature of the pattern dynamics revealed by experiments in injection-driven radial Hele-Shaw flows has been largely underappreciated: although most of the growing fingers split into two, it is not uncommon to find fingers that split by dividing into three others. Therefore, the general tip-splitting events that may occur in existing experiments of radial fingering are not restricted to tip doubling, and split into three fingers (or, tip tripling) is also observed. As opposed to usual tip doubling in which fingers bifurcate at their tips, during tip tripling a trifurcation process takes place, where one observes a single finger dividing into three other smaller fingerlike protrusions. The occurrence of tip tripling can be found, for instance, in the experiments performed in Refs. [2–7] (see Ref. [22] for details). Curiously, in spite of the presence of such trifurcated fingers in these experiments, researchers (experimentalists and theorists) have not paid much attention to them. Maybe this happens because traditional tip-doubling phenomena are considerably more numerous and frequent than their fingertip-tripling counterparts. In any case, the fact is that, regardless of their existence, the study of the development of tip tripling in radial Hele-Shaw cell flows has been largely overlooked in the literature. Similar to the traditional finger doubling events, the finger tripling phenomena are intrinsically nonlinear. In this way, a proper theoretical description of such a still poorly explored situation must go beyond the limitations of purely linear stability analysis.

In this work, we try to fill the gap in literature, and present a theoretical study about the occurrence of fingertip-tripling events in radial Hele-Shaw cell flows. We investigate the early nonlinear regime of pattern formation in radial Hele-Shaw flows under injection, focusing on reproducing the initial stages of the occurrence of fingertip-tripling phenomena. We tackle the problem by employing a perturbative, third-order mode-coupling approach, and by including the contribution of viscous normal stresses into our theoretical description. By doing this, we are able to capture the most relevant morphological aspects of the generated patterned structures which do exhibit the onset formation of both finger doubling, and most importantly, finger tripling structures. Our theoretical results support the idea that normal viscous stresses are an important physical contributor leading to the formation of fingertip-tripling events in radial Hele-Shaw flows induced by injection. Therefore, within the scope of our third-order mode-coupling scheme, the consideration of viscous normal stresses is a necessary theoretical ingredient to allow capturing the emergence of fingertip-tripling events.

We close this section by discussing how our current paper differs from other works that previously studied viscous fingering instabilities while considering the contribution of viscous normal stresses [10,11,20,21]. As mentioned earlier in this introduction, Refs. [20,21] examined the second-order nonlinear dynamics for rotating [20] and injection-induced [21] Hele-Shaw flows. It is worth noting that in rotating Hele-Shaw flows the centrifugally driven fingering structures stretch radially outward and compete among themselves reaching different lengths, but the fingers do not split at their tips. In this manner, fingertip-splitting events of any sort are present, and have not been studied Ref. [20]. Therefore, in contrast to what we do in this work (investigation of normal-stress-mediated tip-tripling phenomena) the main focus in Ref. [20] was on examining how viscous normal stresses affected the characteristic finger competition (or, finger length variability) process. On the other hand, the work carried out in Ref. [21] dealt with radial Hele-Shaw flows, where fingertip splitting does occur. However, as opposed to what we do in this work, Ref. [21] aimed attention at characterizing how viscous normal stresses influenced the development of traditional fingertip doubling, and nothing has been done regarding the occurrence of fingertip tripling.

Another noteworthy difference between the work performed in Refs. [20,21] and here is the fact that while in their studies interesting results can be extracted by a second-order perturbation theory, in our current work we perform a more complete and involved third-order perturbative calculation which allows us to explore the dynamics of the growing interface more accurately. This enables us to have access to even more stimulating nonlinear effects, namely the ones connected to the development of fingertip-tripling structures, a pattern-forming process that has been largely neglected in the literature. It should be stressed that going to third order is actually necessary in order to be able to detect tip tripling while still respecting the validity of the perturbative weakly nonlinear approximation which (i) requires the smallness of the perturbation amplitudes, and (ii) does not allow interface crossings (see Sec. III).

Furthermore, there is one final differing aspect, not only from the weakly nonlinear research performed in Refs. [20,21], but also from the work developed in

Refs. [10,11] which considered the role of viscous normal stresses on Hele-Shaw flow problems, but for purely linear dynamic stages of the flow. The fact is that a key piece of the calculations performed in Refs. [10,11,20,21], precisely the part that adds the contribution of the viscous normal stresses into the problem—the expression for the pressure jump boundary condition—is either incomplete, or in error. The complete and correct expression for such a modified Young-Laplace condition is given in Eq. (7), and derived in Appendix A of this work. It turns out that in Refs. [10,20,21] the authors only considered the action of the radial component of fluid's velocities appearing in the viscous stress tensor (angular velocity components have been neglected). The consideration of a prevalent velocity field contribution along the radial direction is certainly a valid initial approximation, in particular for early time growth. However, the inclusion of azimuthal velocity contributions is necessary at more advanced stages, where nonlinear effects take over. In addition, although the pressure jump condition presented in Ref. [11] [their Eq. (4)] took into account the contributions of both radial and azimuthal components of velocities in the viscous stress tensor, it presents two errors that have been corrected in our Eq. (7).

In summary, our present work expands upon previous research in the field, by addressing a still poorly explored topic in radial Hele-Shaw flows (emergence of tip-tripling events), and by tackling the problem via a more complete and accurate (third-order) perturbative mode-coupling theory. Our theoretical study presents an analysis which was not performed in previous studies, offering ways to predict and detect the most fundamental morphological aspects of the fingertip-tripling phenomenon in radial Hele-Shaw flows.

II. THEORETICAL FORMULATION AND THE THIRD-ORDER MODE-COUPLING EQUATION

Consider the motion of two Newtonian, immiscible, incompressible viscous fluids, flowing in a narrow gap of thickness b that separates two parallel glass plates of a circular Hele-Shaw cell. The viscosities of the inner and outer fluids are denoted as η_1 and η_2, respectively. Fluid 1 is injected into fluid 2 through a small orifice located at the center of the cell, at a constant flow rate Q, which is the area covered per unit time. At the fluid-fluid interface there is a surface tension σ. Within the framework of our perturbative mode-coupling theory, the deformed two-fluid interface is described as

$$\mathcal{R}(\theta, t) = R(t) + \zeta(\theta, t), \tag{1}$$

where $|\zeta| \ll R$, θ represents the azimuthal angle, and $R(t) = \sqrt{R_0^2 + (Q/\pi)t}$ is the time-dependent unperturbed radius of the evolving interface, with R_0 being the unperturbed interface radius at $t = 0$. In Eq. (1)

$$\zeta(\theta, t) = \sum_{n=-\infty}^{+\infty} \zeta_n(t) \exp(in\theta) \tag{2}$$

is the perturbation amplitude, where $\zeta_n(t)$ denotes the complex Fourier mode amplitudes, and n is the integer azimuthal wave number. Mass conservation imposes that the zeroth mode is written in terms of the other modes as $\zeta_0 = -(1/2R) \sum_{n \neq 0} |\zeta_n(t)|^2$ [17]. We are interested in the early

nonlinear behavior of the system, specifically in the development of fingertip tripling, by taking into account the contribution of viscous normal stresses. Therefore, our main task in this section is to derive a mode-coupling differential equation which describes the time evolution of the perturbation amplitudes $\zeta_n(t)$, accurate to third order.

The governing equations for the system are Darcy's law [1],

$$\mathbf{v}_j = -\frac{b^2}{12\eta_j} \nabla p_j, \tag{3}$$

and the continuity equation for incompressible fluids,

$$\nabla \cdot \mathbf{v}_j = 0, \tag{4}$$

where $\mathbf{v}_j = \mathbf{v}_j(r, \theta)$ and $p_j = p_j(r, \theta)$ denote the gap-averaged velocity and pressure in fluids $j = 1$ and 2, respectively.

From the irrotational nature of the flow in Hele-Shaw cells, one can define a velocity potential ϕ_j, where $\mathbf{v}_j = -\nabla \phi_j$. The equation of motion for the perturbed fluid-fluid interface $r = \mathcal{R}$ can be obtained by rewriting Darcy's law [Eq. (3)] in terms of the velocity potential for each fluid, and then by subtracting the resulting expressions, yielding

$$A\left(\frac{\phi_1 + \phi_2}{2}\right) - \left(\frac{\phi_1 - \phi_2}{2}\right) = -\frac{b^2(p_1 - p_2)}{12(\eta_1 + \eta_2)}, \tag{5}$$

where

$$A = \frac{\eta_2 - \eta_1}{\eta_2 + \eta_1} \tag{6}$$

is the viscosity contrast (a dimensionless viscosity difference) which varies in the range $-1 \leqslant A \leqslant 1$. For the Saffman-Taylor problem under radial injection, the interface is unstable only for $A > 0$. Throughout this work, consistent with previous studies on this research topic [1–7], we focus on the most unstable situation in which $A = 1$. In addition, notice that the velocity potentials obey Laplace's equation $\nabla^2 \phi_j = 0$.

The problem is then specified by two boundary conditions. The first one is a modified pressure jump, Young-Laplace condition which incorporates the role of viscous normal stresses,

$$\begin{aligned}
p_1 - p_2 = \sigma\kappa - 2\delta\eta_1 &\left[n_r^2 \frac{\partial^2 \phi_1}{\partial r^2} + 2n_r n_\theta \left(\frac{1}{r} \frac{\partial^2 \phi_1}{\partial r \partial \theta} - \frac{1}{r^2} \frac{\partial \phi_1}{\partial \theta} \right) \right. \\
&\left. + n_\theta^2 \left(\frac{1}{r^2} \frac{\partial^2 \phi_1}{\partial \theta^2} + \frac{1}{r} \frac{\partial \phi_1}{\partial r} \right) \right] + 2\delta\eta_2 \left[n_r^2 \frac{\partial^2 \phi_2}{\partial r^2} \right. \\
&+ 2n_r n_\theta \left(\frac{1}{r} \frac{\partial^2 \phi_2}{\partial r \partial \theta} - \frac{1}{r^2} \frac{\partial \phi_2}{\partial \theta} \right) \\
&\left. + n_\theta^2 \left(\frac{1}{r^2} \frac{\partial^2 \phi_2}{\partial \theta^2} + \frac{1}{r} \frac{\partial \phi_2}{\partial r} \right) \right], \tag{7}
\end{aligned}$$

where κ is the interface curvature in the plane of the cell. As in Refs. [10,11,20,21], in Eq. (7) the curvature of the fluid-fluid interface across the width of the cell is not accounted for. This nearly constant transverse curvature is set by the static contact angle measured between the plates and the curved meniscus (assumed to be circular with radius $b/2$). Since its gradient is nearly zero, this transverse curvature does not significantly affect the motion in our Darcy's law regulated

problem [1,2]. In Eq. (7) the parameter δ is used to keep track of the contributions coming from the viscous normal stresses: $\delta = 0$ if normal stresses are neglected, and $\delta = 1$ if normal stresses are taken into account. In addition, n_r and n_θ denote the radial and azimuthal components of the unit normal vector to the interface. A derivation of Eq. (7) is given in Appendix A. We emphasize that our Eq. (7) differs a bit from the equivalent expression originally obtained in Ref. [11] [see their Eq. (4)] which is not entirely correct. Their expression misses the factors of 2 which multiply the terms $n_r n_\theta$ on the right hand side of Eq. (7).

The second relevant boundary condition is the so-called kinematic boundary condition [1],

$$\frac{\partial \mathcal{R}}{\partial t} = \left[\frac{1}{r^2} \frac{\partial r}{\partial \theta} \frac{\partial \phi_j}{\partial \theta} - \frac{\partial \phi_j}{\partial r} \right]_{r=\mathcal{R}}, \qquad (8)$$

which expresses the fact that the normal components of each fluid's velocity are continuous at the interface.

To conclude our derivation of the mode-coupling differential equation that describes the time evolution of the interfacial amplitudes $\zeta_n(t)$, we follow standard steps performed in previous weakly nonlinear studies [17–21]. First, we define Fourier expansions for the velocity potentials and use the kinematic boundary condition [Eq. (8)] to relate the velocity potential Fourier amplitudes to $\zeta_n(t)$ and $\dot{\zeta}_n(t) = d\zeta_n/dt$. Substituting these relations, and the modified pressure jump condition Eq. (7) into Eq. (5), always keeping terms up to third order in ζ, and Fourier transforming, we find the *dimensionless* equation of motion for the perturbation amplitudes (for $n \neq 0$),

$$\dot{\zeta}_n = \lambda(n)\zeta_n + \sum_p \{[F(n, p) + S_F(n, p)]\zeta_p \zeta_{n-p} + [G(n, p) + S_G(n, p)]\dot{\zeta}_p \zeta_{n-p}\}$$

$$+ \sum_{p,q} \{[H(n, p, q) + S_H(n, p, q)]\zeta_p \zeta_{n-q}\zeta_{q-p} + [I(n, p, q) + S_I(n, p, q)]\dot{\zeta}_p \zeta_{n-q}\zeta_{q-p}$$

$$+ [J(n, p, q) + S_J(n, p, q)]\zeta_p \zeta_q \zeta_{n-p-q} + [K(n, p, q) + S_K(n, p, q)]\dot{\zeta}_p \zeta_q \zeta_{n-p-q}\}, \qquad (9)$$

where

$$\lambda(n) = \frac{1}{s(n)} \left\{ \frac{1}{2\pi R^2} \left[A|n| \left(1 + \delta \frac{1}{3R^2} \right) - s(n) \right] \right.$$

$$\left. - \frac{(A+1)}{2CaR^3} |n|(n^2 - 1) \right\} \qquad (10)$$

is the linear growth rate,

$$Ca = \frac{12\eta_2 Q}{\sigma b} \qquad (11)$$

is the global capillary number which expresses a relative measure of viscous to surface tension forces, and

$$s(n) = 1 + \delta \frac{1}{6R^2} |n|(|n| + A). \qquad (12)$$

The global capillary number Ca [Eq. (11)] is an important control parameter of our radial Hele-Shaw cell system and should be distinguished from the local (or instantaneous) capillary

number $\overline{Ca} = \eta \dot{R}/\sigma$ (η is the viscosity of the displaced fluid) which can be orders of magnitude smaller [1,23]. Typical values of the local capillary number used in radial Hele-Shaw cell experiments vary within a widespread range $O(10^{-4}) \leqslant \overline{Ca} \leqslant O(10^2)$ [1–7]. In these very same studies, the typical values of the global capillary number vary within a shorter range $O(10) \leqslant Ca \leqslant O(10^3)$.

The long and somewhat complicated expressions for the nonlinear mode-coupling functions F, S_F, G, S_G, H, S_H, I, S_I, J, S_J, K, and S_K are given in Appendix B—see Eqs. (B1)–(B14). In Eq. (9) lengths are rescaled by b, and velocities by Q/b. From now on, we work with the dimensionless version of the equations. We emphasize that to strengthen the reliability and soundness of our theoretical results, the values of all dimensionless parameters we use throughout this work are consistent with typical physical quantities used in real experiments in radial Hele-Shaw flows driven by injection [2–7].

For a truly consistent third-order expression, we replace the time derivative terms $\dot{\zeta}_p$ appearing on the right hand side of Eq. (9) by $\lambda(p)\zeta_p + O(\zeta^2)$, to finally obtain

$$\dot{\zeta}_n = \lambda(n) \zeta_n + \sum_{p \neq 0} \{F(n, p) + S_F(n, p) + \lambda(p)[G(n, p) + S_G(n, p)]\} \zeta_p \zeta_{n-p}$$

$$+ \sum_{p,q \neq 0} \{[H(n, p, q) + S_H(n, p, q) + \lambda(p)[I(n, p, q) + S_I(n, p, q)]$$

$$+ [G(n, q) + S_G(n, q)]\{F(q, p) + S_F(q, p) + \lambda(p)[G(q, p) + S_G(q, p)]\}] \zeta_p \zeta_{q-p} \zeta_{n-q}$$

$$+ [J(n, p, q) + S_J(n, p, q) + \lambda(p)(K(n, p, q) + S_K(n, p, q))] \zeta_p \zeta_q \zeta_{n-p-q}\}. \qquad (13)$$

This is the third-order mode-coupling equation for the injection-driven flow problem in a radial Hele-Shaw cell, tak-

ing into consideration the action of viscous normal stresses. By inspecting Eq. (13) it is evident that the third-order terms

add extra complexity to the description of the problem. However, the inclusion of these higher-order terms are necessary to provide a more thorough description of the interface dynamics than previous first- and second-order approaches to the problem [11,21]. Even higher perturbative orders [$O(\zeta_n^4)$, $O(\zeta_n^5)$, etc.] are not considered since, due to the smallness of ζ_n with respect to R ($|\zeta_n| \ll R$), their contributions for the interface dynamics become unimportant.

III. DISCUSSION

In this section, our perturbative mode-coupling theory is utilized to investigate the possibility of describing the development of fingertip-tripling events at early nonlinear stages of confined, injection-driven radial flows. We do that by considering the action of viscous normal stresses. To carry out this task, we make use of the third-order differential equation for the perturbation amplitudes [Eq. (13)], and rewrite the complex interfacial perturbation given in Eq. (2) in terms of cosine and sine modes,

$$\zeta(\theta, t) = \zeta_0 + \sum_{n=1}^{\infty}[a_n(t)\cos n\theta + b_n(t)\sin n\theta], \qquad (14)$$

where $a_n(t) = \zeta_n(t) + \zeta_{-n}(t)$, and $b_n(t) = i[\zeta_n(t) - \zeta_{-n}(t)]$ are real valued. In Eq. (14) we include the mode $n = 0$ to maintain the area of the perturbed shape independent of the perturbation ζ. By applying such area conservation constraint, the zeroth mode amplitude can be conveniently expressed in terms of the other modes $n \geqslant 1$ as [17]

$$\zeta_0 = -\frac{1}{4R}\sum_{n=1}^{\infty}\left[a_n^2(t) + b_n^2(t)\right]. \qquad (15)$$

To reproduce the actual shape of the growing interface patterns, we consider the nonlinear coupling of a finite number of Fourier modes, and from Eq. (13) obtain the corresponding mode-coupling differential equations for the mode amplitudes $a_n(t)$ and $b_n(t)$. The time evolution for $a_n(t)$ and $b_n(t)$ gives the time evolution for the interface itself [from Eqs. (1) and (14)]. The resulting set of coupled nonlinear differential equations for these real valued amplitudes is solved in MATLAB, using an explicit Runge-Kutta scheme for nonstiff problems with absolute and relative tolerances set to 10^{-4} [24,25]. A sensitivity analysis was performed to guarantee convergence of the solutions.

It has been shown [17] that the classical tip-splitting mechanism resulting in tip doubling in radial Hele-Shaw flows can be consistently mimicked by considering the weakly nonlinear coupling of just two particularly relevant Fourier modes: a fundamental mode n, and its first-harmonic mode $2n$. So, within the scope of such a simplified perturbative mode-coupling scheme, tip-doubling phenomena would be produced as the result of the influence of mode n on the growth of mode $2n$. In this picture, the fundamental mode sets the overall n-fold symmetry of the pattern, while the first harmonic mode $2n$ determines the shape of the fingertip (i.e., if it is sharp, wide, or even if it splits). By analogy, if on top of conventional tip doubling, one wishes to study the possible occurrence of fingertip tripling, the simplest alternative would be to examine the interface growth by considering the nonlinear

interplay of modes n, $2n$, and $3n$. In the realm of this idealized mode-coupling picture with a few participating modes, it is plausible to assume that tip-tripling formation would require the presence of mode $3n$. To better appreciate the nonlinear results that may emerge under this simplified mode-coupling approach involving only modes n, $2n$, and $3n$, we analyze Fig. 1.

In the top panels of Fig. 1, we depict the fluid-fluid interface time evolution for $0 \leqslant t \leqslant t_f$ considering the interaction of the Fourier modes n, $2n$, and $3n$. This is done by taking the following characteristic dimensionless parameter values: $A = 1$, Ca $= 200$, and $R_0 = 3$. The interfaces are plotted in equal time intervals $\Delta t = t_f/10$, where t_f is the final time. Moreover, in the bottom panels of Fig. 1, we display the corresponding time evolution of the rescaled perturbation amplitudes $|\zeta_n(t)|/R(t)$, where $|\zeta_n(t)| = \sqrt{a_n^2(t) + b_n^2(t)}/2$, for each of the modes.

As mentioned earlier, we make sure that the representative dimensionless parameters we utilize (A, Ca, and R_0) are fully compatible with the values of the relevant physical quantities used in real experimental studies in radial Hele-Shaw flows [2–7]. In these experimental studies researchers use a variety of values for the physical quantities involved in the problem. Typical values for these quantities are injection flow rates 0.2 cm^2/s $\leqslant Q \leqslant 150$ cm^2/s, surface tension ranging 20-65 dyne/cm, cell gap thickness 0.075 cm $\leqslant b \leqslant 0.15$ cm, and initial radius R_0 from 0.5 to 5 cm. A number of different fluid viscosities are utilized for both fluids, but to maximize interface deformations many experimental runs operate in the highest viscosity contrast limit, where an inner fluid of negligible viscosity ($\eta_1 \approx 0$, for instance, air, nitrogen, etc.) displaces a viscous oil (for example, some type of glycerin or silicone oil) of viscosity η_2 ranging 1–10 g/cm s. In this framework, one can say that the dimensionless parameters $O(10) \leqslant$ Ca $\leqslant O(10^3)$ and $O(1) \leqslant R_0 \leqslant O(10)$. Moreover, for unstable displacements of the interface one has that $0 < A \leqslant 1$.

The particular choice we make for the viscosity contrast ($A = 1$) is motivated by its vast use in experiments, and also because it considerably favors interface destabilization. On the other hand, the use of a capillary number of moderate intensity (Ca $= 200$) is justified by the fact that we wish to avoid an abrupt, exaggerated growth of the interface, something that would put us very quickly in a regime in which our perturbative model could not be applied. There is nothing really special about the value for R_0 we take, other than it lies within of the range of typical values used in experiments.

Throughout this work, to further guarantee the validity of the perturbative solutions, while depicting the evolving interfaces, we stop the time evolution of the patterns as soon as the base of the fingers starts to move inward, which would cause successive interfaces to cross one another [26]. Since this crossing is not observed in radial Hele-Shaw cell experiments [1–7], the largest time before crossing is used as the upper bound time ($t = t_f$) for the applicability of our perturbative description. In addition, consistent with our perturbative scheme, in all situations examined in this work we require that $|\zeta_n(t)|/R(t) \ll 1$. As a matter of fact, we make sure that all perturbation amplitudes $|\zeta_n(t)|$ we obtain are always well below 10% of $R(t)$.
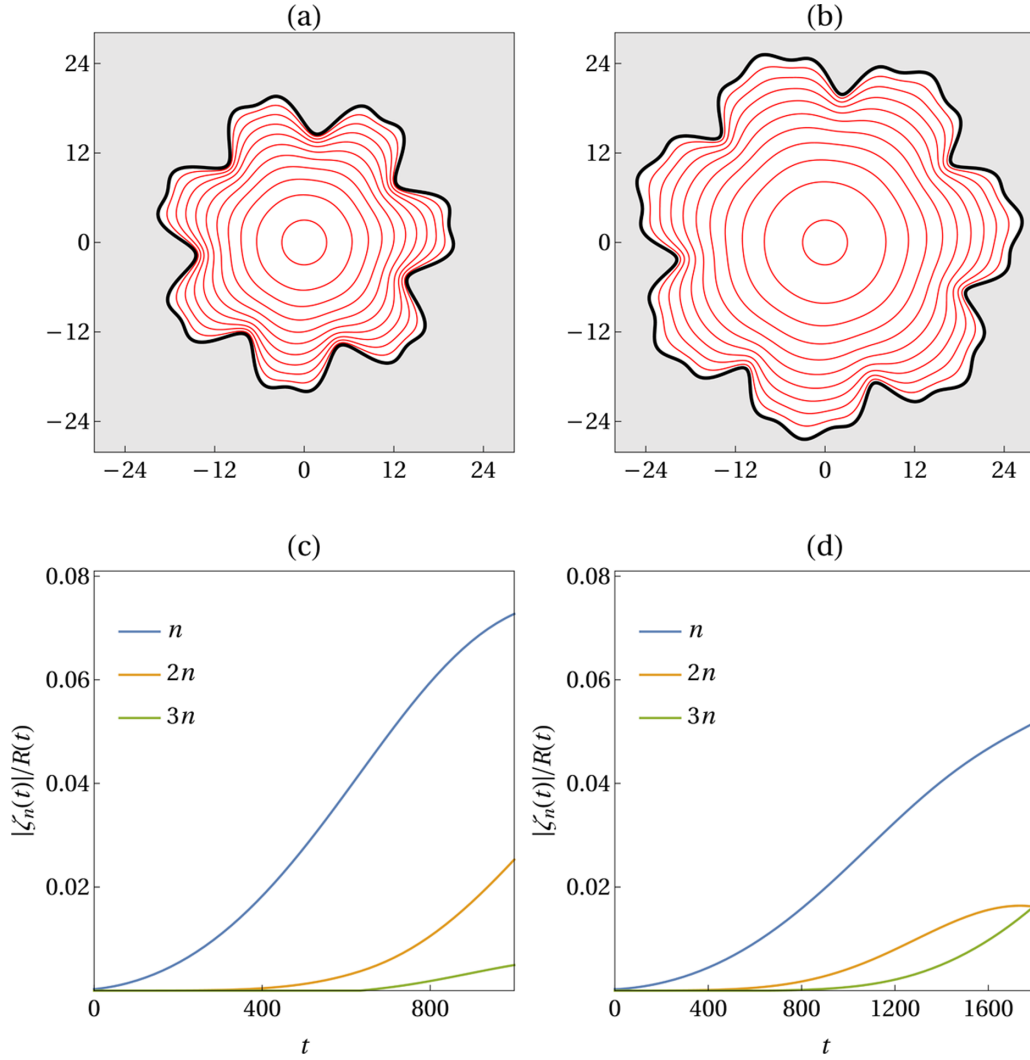
FIG. 1. Time evolution of the interfacial patterns generated by solving Eq. (13) for $0 \leqslant t \leqslant t_f$ when (a) $\delta = 0$ and $t_f = 1000$, (b) $\delta = 1$ and $t_f = 1800$. The time t_f is the maximum allowed time before interface crossings begin. Here we consider the third-order nonlinear coupling of the fundamental mode $n = n_{\max}^{\zeta} = 7$, with its harmonics $2n = 14$ and $3n = 21$. The corresponding time evolution of the rescaled perturbation mode amplitudes $|\zeta_n(t)|/R(t)$ are illustrated in (c) for $\delta = 0$, (d) for $\delta = 1$. The flow parameters are $A = 1$, $Ca = 200$, and $R_0 = 3$. The initial perturbation amplitudes are $a_n(0) = b_n(0) = R_0/2500$, and $a_{2n}(0) = b_{2n}(0) = a_{3n}(0) = b_{3n}(0) = 0$.

To plot Fig. 1, we follow Ref. [27], and choose the fundamental mode n to be the mode of largest amplitude, as given by linear stability analysis. From the purely linear terms of Eq. (13), one can readily see that the linear perturbation amplitude is given by

$$\zeta_n(t) = \zeta_n(0) \exp\left[\int_0^t \lambda(n)dt\right], \quad (16)$$

with $\zeta_n(0)$ being the interfacial amplitude at $t = 0$. The mode of maximum amplitude ($n_{\max}^{\zeta}$) is thus obtained by maximizing the interfacial amplitude (16),

$$\left(\frac{d\zeta_n(t)}{dn}\right)\bigg|_{n=n_{\max}^{\zeta}} = 0. \quad (17)$$

It has been shown in Ref. [27] that $n_{\max}^{\zeta}$ is a better predictor for the number of fingers generated at the linear regime than the mode corresponding to the maximum of the growth rate ($n_{\max}^{\lambda}$) which is obtained by setting $[d\lambda(n)/dn]_{n=n_{\max}^{\lambda}} = 0$. Therefore,

we consider the fundamental mode $n = n_{\max}^{\zeta}$ taken at time t_f. For the circumstances considered in Fig. 1 $n = n_{\max}^{\zeta} = 7$, therefore $2n = 14$ and $3n = 21$. To make sure that the interfacial behaviors we portray in Fig. 1 are spontaneously induced by the weakly nonlinear dynamics, and not by artificially imposing large initial amplitudes for the harmonic modes $2n$ and $3n$ modes, we set the initial ($t = 0$) harmonic mode amplitudes to zero. Therefore, at $t = 0$ only the fundamental mode n has nonzero, but small amplitudes $a_n(0) = b_n(0) = R_0/2500$.

We begin our discussion by examining Figs. 1(a) and 1(c) which focus on the case where viscous normal stresses are neglected ($\delta = 0$), and $t_f = 1000$. In Fig. 1(a) we observe a nearly circular initial interface evolving to a seven-fingered structure. As time progresses, we notice the development of fingertip widening, followed by a fingertip-flattening process. At later times, one then sees the emergence of fingertip splitting, via tip doubling. These morphological observations are backed up by what we see in Fig. 1(c) for the growth of the perturbation amplitudes: the overall sevenfold shape is

determined by the growth of the fundamental mode $n = 7$, while the fingertip widening, flattening, and doubling are induced by the enhanced growth of the first harmonic mode $2n = 14$. These remarks are consistent with the theoretical findings of Refs. [17,21], and with the experimental results of Refs. [1–7] with respect to the occurrence of usual tip-splitting behavior, leading to tip doubling. It is worth pointing out that there is no sign of tip tripling in Fig. 1(a), in consonance with what is observed in Fig. 1(c) which shows that mode $3n = 21$ has a small amplitude when $\delta = 0$.

Now we turn our attention to Figs. 1(b) and 1(d) where the influence of viscous normal stresses is taken into account ($\delta = 1$), and $t_f = 1800$. Notice that $t_f = 1800$ for $\delta = 1$, while $t_f = 1000$ for $\delta = 0$. This happens because viscous normal stresses exert a stabilizing role, and slow down the growth of the pattern as a whole. Therefore, for $\delta = 1$ one can evolve the dynamics to larger times, still conveniently avoiding the prohibited crossing between successive interfaces. This overall stabilizing effect introduced by the normal stress is quite general, and in accordance with the findings of Refs. [10,11,20,21].

It is evident that the patterned structure depicted in Fig. 1(b) for $\delta = 1$ is different from the shape illustrated in Fig. 1(a) for $\delta = 0$. One can clearly see that the prevalent morphological feature in Fig. 1(b) is not fingertip doubling, but tip tripling. Indeed, in Fig. 1(b) we see an initially sevenfold structure which evolves towards a 21-fold fingered morphology. The rising of fingertip-tripling phenomena for the pattern evolution that includes the presence of viscous normal effects can be justified by inspecting Fig. 1(d), where we see the growth of a sizable amplitude for mode $3n$. By contrasting the growth of mode $3n$ in Figs. 1(c) and 1(d) one finds that the final amplitude of mode $3n$ significantly increases under the presence of viscous normal stresses. Moreover, in Fig. 1(d), although we observe that mode n still reaches a larger amplitude than mode $3n$, the growth of mode $2n$ is clearly inhibited. The combination of these factors leads to the emergence of fingertip-tripling events.

By comparing Figs. 1(a) and 1(b), one can also notice that the pattern with stress has a larger size. This is due to the stabilizing effects of normal stresses mentioned earlier, making the pattern with stress larger than its counterpart that neglects it. This finding can be further evidenced by scrutinizing Figs. 1(c) and 1(d), where one can verify that the amplitude for the fundamental mode n is attenuated when stresses are present. Therefore, when the influence of normal stresses is taken into account ($\delta = 1$), the result is the emergence of a larger pattern for which the fingers are wider (effect related to the growth of mode $2n$ at earlier times), with their tips splitting into three small lobes (due to the enhanced growth of mode $3n$). This indicates that the formation of tip tripling involves the nonlinear coupling of both modes $2n$ and $3n$ in which the growing finger first becomes wider due to the growth of mode $2n$, and then branches out into three small lobes as a consequence of the enhanced nonlinear growth of mode $3n$. These observations hint at a third-order weakly nonlinear mechanism leading to the emergence of fingertip tripling when modes n, $2n$, and $3n$ are present.

The theoretical results for the time evolution of patterns and mode amplitudes under the absence ($\delta = 0$) and presence

($\delta = 1$) of viscous normal stresses illustrated in Fig. 1 indicate that the consideration of these stresses favor the occurrence of fingertip-tripling phenomena. However, the scenario contemplated in Fig. 1 is somewhat optimized, in the sense that only three particular modes are present, and specific initial conditions are considered, leading to the formation of very symmetric n-fold structures for which only tip doubling (for $\delta = 0$) or tip tripling (for $\delta = 1$) ultimately emerge as prevalent morphological features.

From now on, our primary goal is to test the basic morphological outcomes revealed by Fig. 1, but trying to verify the robustness of such results under more realistic circumstances. To do that we follow a successful model proposed in Ref. [28] by Cardoso and Woods for evolving interfaces in the linear regime (their "model B"), and extended in Ref. [17] to the weakly nonlinear stage. This model is in line with typical circumstances of real experiments in radial Hele-Shaw flows [1–7], and explores the effect of a background level of noise on the dynamics of the interface. The possible sources of noise may come, for example, from irregularities in the gap thickness b, inhomogeneities on the surface of the Hele-Shaw cell, or even from thermal or pressure fluctuations [26]. Taking these issues under consideration, the model describes the behavior of the two-fluid interface assuming the presence of a constant low level of noise during its entire evolution. In this framing, each participating Fourier mode n is perturbed with a constant (in time) random complex amplitude $\zeta_n(0)$ which contains an n dependent random phase, whose magnitude $|\zeta_n(0)|$ is independent of n by assumption. As the interface advances radially, it successively reaches critical radii $R_c(n)$ [obtained by setting $\lambda(n) = 0$] for each mode n, such that only once a particular $R_c(n)$ is reached, the perturbation amplitude ζ_n starts to vary with time. The predictions of this model are in good agreement with experimental observations within the linear [28] and weakly nonlinear [17] regimes.

Furthermore, in all the patterns presented in the rest of this study, we will not be restricted to include only a few participating modes, but more sensibly consider the participation of all Fourier modes which lie within the band of unstable modes at time $t = t_f$. Unless otherwise stated, as we also did in plotting Fig. 1, in the remainder of this work we continue to consider a representative set of dimensionless parameters Ca, A, R_0 which are in consonance with physical values commonly used in many radial Hele-Shaw cell experiments [1–7]. Moreover, in Figs. 2–7 we take the noise amplitude $|\zeta_n(0)| = R_0/1500$.

Under these circumstances, we consider the participation of the Fourier modes $2 \leqslant n \leqslant 21$. Recall that the mode $n = 0$ is written in terms of the other modes via Eq. (15), and note from Eq. (10) that since $-1 \leqslant A \leqslant 1$, the mode $n = 1$ (which corresponds to a rigid translation of a circular interface) is either linearly stable $\lambda(n = 1) < 0$, or marginal $\lambda(n = 1) = 0$. These facts are true for both $\delta = 0$ and $\delta = 1$. Although we illustrate our main results by focusing on a representative set of parameters, the reproducibility of the results is tested generating them by using different initial conditions, in particular by changing the random phases attributed to each mode [17,26,28]. By doing this we can verify the robustness of our weakly nonlinear results if such conditions are changed. At
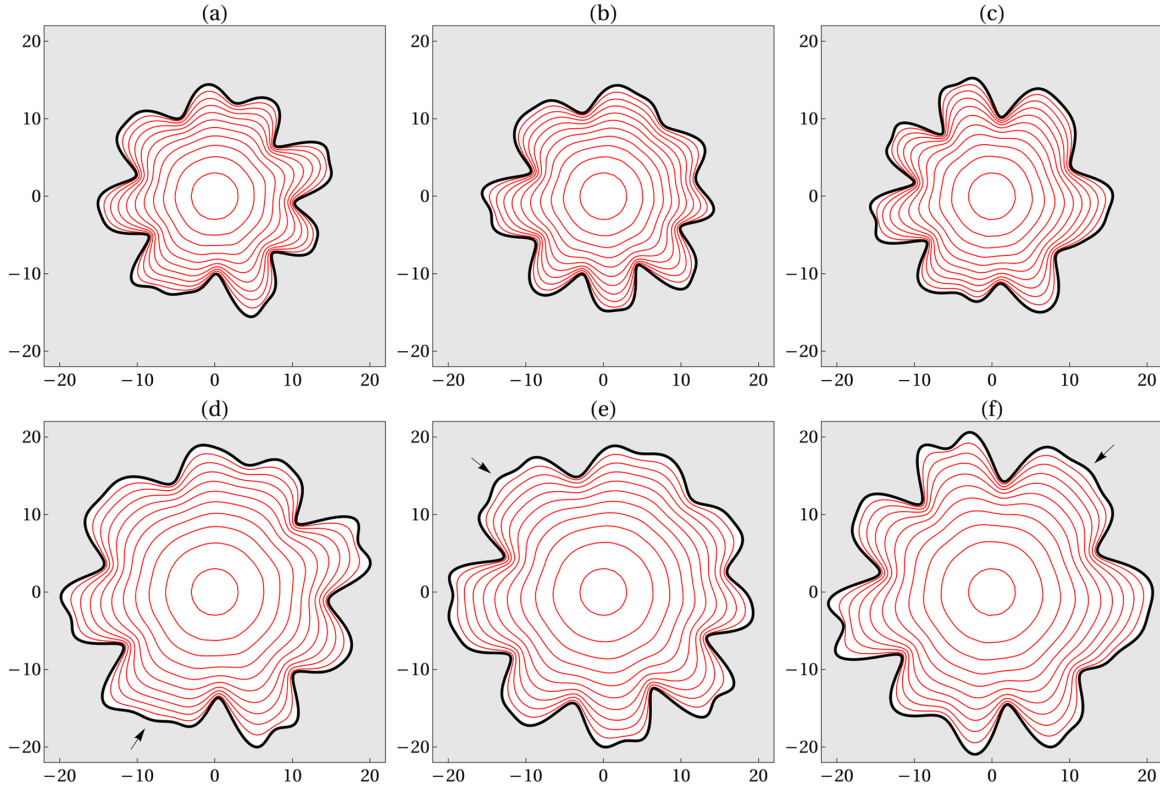
FIG. 2. Time evolution of the interfacial patterns generated by solving Eq. (13) for $2 \leqslant n \leqslant 21$, $0 \leqslant t \leqslant t_f$ and equal time intervals $\Delta t = t_f/10$, considering (a)–(c) $\delta = 0$ and (d)–(f) $\delta = 1$. The values of t_f are (a) 530, (b) 530, (c) 560, (d) 970, (e) 1012, and (f) 1060. Three different sets of random phases are used, one for (a) and (d), a second for (b) and (e), and a third for (c) and (f). The occurrence of tip-tripling events in (d)–(f) is indicated by small arrows. Here $A = 1$, Ca $= 200$, and $R_0 = 3$.

the end of this section, we also examine how changes in the controlling parameters Ca and A may alter the development of fingertip-tripling events.

Keeping in mind the important information given in the previous two paragraphs, in Fig. 2 we plot the third-order interface evolution, for a whole range of participating modes $2 \leqslant n \leqslant 21$, when viscous normal stresses are neglected [(a)–(c) for $\delta = 0$], and taken into account [(d)–(f) for $\delta = 1$]. To lend support to our theoretical results, three distinct sets of random phases are examined, a first one for (a) and (d), a second for (b) and (e), and a third for (c) and (f). By going through Figs. 2(a)–(c), we observe the formation of typical viscous fingering patterns in which seven or eight main fingers of various sizes grow. Interestingly, considering the parameters of the problem, one finds that $7 \leqslant n_{\max}^{\zeta} \leqslant 8$, while $12 \leqslant n_{\max}^{\lambda} \leqslant 13$, demonstrating that $n_{\max}^{\zeta}$ is a better indicator for the number of fingers formed. One can also notice that some of the fingers tend to get increasingly wider, and flatter at their tips as time advances. In particular, one can notice that some of the flattened tip fingers begin to split via a tip-doubling process. However, in these cases in which normal stresses are neglected one does not verify the development of fingertip tripling.

On the other hand, by analyzing Figs. 2(d)–(f), one perceives a somewhat different sequence of events. When normal stresses are included one also finds the emergence of characteristic fingering patterns, where finger widening, flattening, and splitting occur. It is curious to note that under the ac-

tion of normal stresses the fingers look a little shorter and stubbier than the corresponding fingered structures observed when such stresses are neglected [Figs. 2(a)–(c)]. This last observation is a consequence of the stabilizing effect induced by the viscous normal stresses, which has the tendency to slow down interfacial pattern growth. Given the increased stability, note that t_f is bigger for $\delta = 1$. However, the most peculiar morphological aspect that arises when normal stresses act is the existence of fingers which display the onset of tip-tripling events. To better guide the eye, these three-fingered structures are indicated by small arrows in Figs. 2(d)–(f). Of course, fingertip doubling is also detected when $\delta = 1$. As anticipated by the simplified scenario discussed in Fig. 1, in Figs. 2(d)–(f) once again we identify the formation of fingertip tripling induced by the action of viscous normal stresses. We emphasize that, different from what happened in Fig. 1, where only three predetermined modes compete and interact in the absence of noise, in Figs. 2(d)–(f) tip-tripling events persist under much more realistic circumstances, despite the presence of a full range of linearly unstable competing modes, and the action of random noise.

It is worth noting that we have verified what would happen to the patterns if all parameters and initial conditions are kept as the ones used in Fig. 2, but if we use second-order and not third-order theory to generate them. We have found that these second-order patterns do not present the emergence of fingertip tripling. As a matter of fact, this very same observation is also valid for the third-order patterns illustrated in Figs. 6
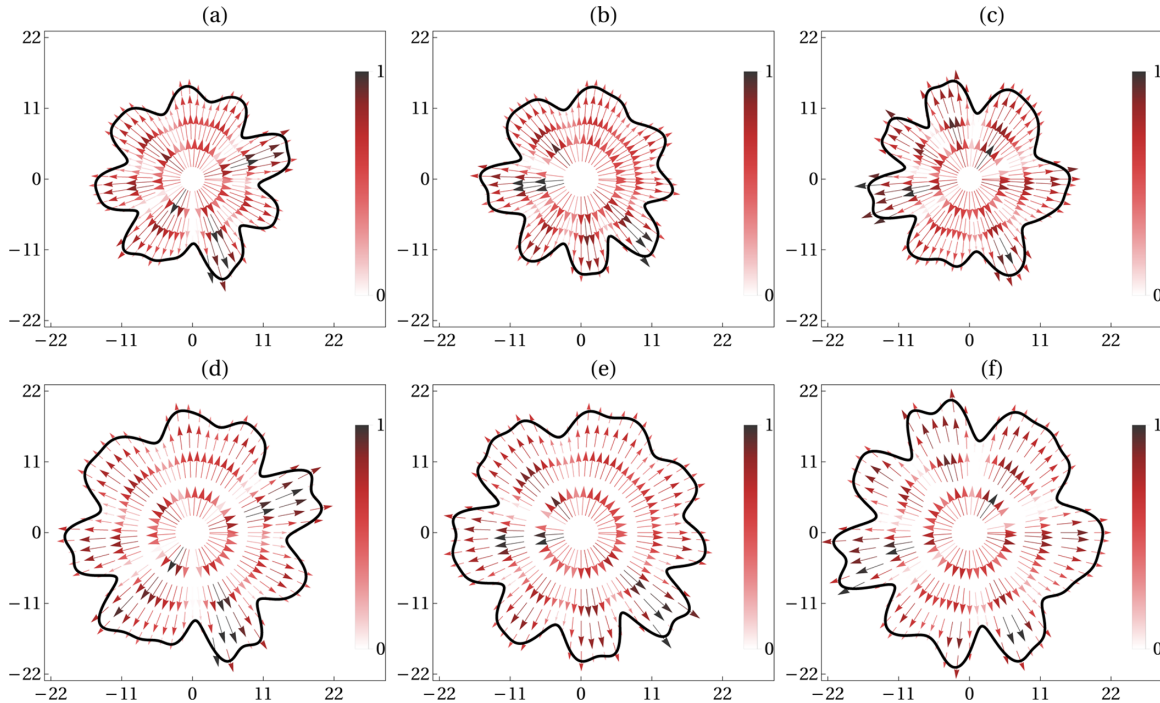
FIG. 3. Snapshots of the velocity fields for the interface evolutions portrayed in Fig. 2, overlaid with the corresponding interface shapes taken at final times $t = t_f$. Note that (a)–(c) $\delta = 0$ and (d)–(f) $\delta = 1$. All physical parameters, initial conditions, and random phases are the same as those used in Fig. 2. Darker colors and larger size arrows indicate higher local velocities. As in Fig. 2 $A = 1$, Ca $= 200$, and $R_0 = 3$.

and 7 (i.e., their second-order counterparts do not show any tip tripling).

Complementary information about the interface time evolution behaviors observed in Fig. 2 is explored in a bit more quantitative fashion in Figs. 3 and 4. Figure 3 represents the velocity vector fields taken from the time evolutions portrayed in Fig. 2 and the associated two-fluid interface shapes evaluated at final times $t = t_f$. The color coding is such that darker colors and larger arrows indicate higher local velocities. By examining Fig. 3, and contrasting the situations without [(a)–(c) for $\delta = 0$] and with [(d)–(f) for $\delta = 1$] viscous normal stresses, one can see that the presence of such viscous stresses influences the resulting velocity field disposition, changing the speed of propagation of the interface. The stresses delay the growth of perturbations, allowing the fingers to propagate for longer times, and to get wider at their tips, ultimately favoring the development of both fingertip-doubling and tip-tripling phenomena.

Another relevant piece of information is provided by Fig. 4. It depicts the time evolution of the rescaled perturbation amplitudes $|\zeta_n(t)|/R(t)$, where $|\zeta_n(t)| = \sqrt{a_n^2(t) + b_n^2(t)}/2$ for each of the participating Fourier modes $2 \leqslant n \leqslant 21$ associated with the interfacial pattern growths illustrated in Fig. 2. By comparing the growth of the perturbation amplitudes by neglecting [(a)(c) for $\delta = 0$] and considering [(d)–(f) for $\delta = 1$] the influence of viscous normal stresses, one can readily see that stresses considerably impact the amplitudes' time evolution behavior, leading to a significant attenuation of their growth. This more quantitative finding is in line with our more visual observations regarding the shorter and thicker nature of the resulting fingers under the presence of stress, and with the possibility of evolving the patterns up until longer times

when stresses are included. Ultimately, our third-order mode-coupling findings reveal a dual role played by viscous normal stresses regarding interface growth in radial Hele-Shaw flows: if on one hand stresses act to restrain the overall growth of the patterns, on the other hand they modify the local velocity field in such a way that the growth of tip-splitting events (including both tip doubling, and tip tripling) is stimulated.

Up to this point, we have illustrated our results on the development of fingertip-tripling phenomena induced by viscous normal stresses, for representative values of the viscosity contrast, and capillary number, namely for $A = 1$, and Ca $= 200$. To check how the evolving interface responds to changes in these two fundamental parameters, we examine what happens if other characteristic values of A and Ca are considered. Before proceeding, we call the reader's attention to the role played by these key parameters in injection-driven radial Hele-Shaw flows. It is well known that, no matter whether normal stresses are taken into consideration or not, increasingly larger values of A and Ca tend to destabilize the system [2–7,11,21]. So far, we have focused on the situation of maximum instability regarding the viscosity contrast ($A = 1$). Nevertheless, in principle, for unstable interface displacements one can have $0 < A \leqslant 1$. On the other hand, the capillary number may vary within a wide spread range of values in radial Hele-Shaw experiments: typically $O(10) \leqslant$ Ca $\leqslant O(10^3)$. If Ca is too small the interface is quite stable against perturbations, making its time evolution uninteresting. However, if Ca is very large the interface becomes very quickly deformed, creating difficulties for an accurate early nonlinear theoretical description, since the undesired (and unphysical) interface crossings occur rapidly.
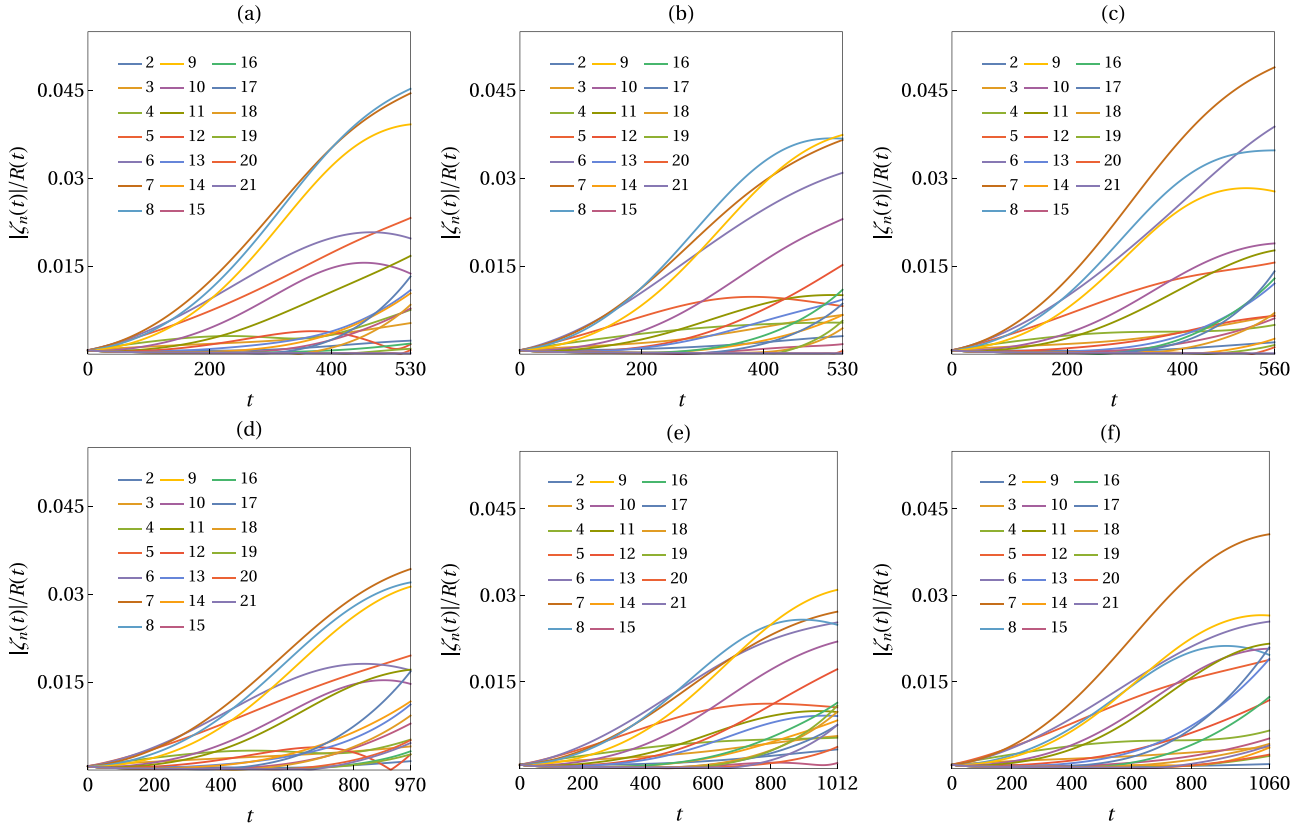
FIG. 4. Time evolution of the rescaled perturbation mode amplitudes $|\zeta_n(t)|/R(t)$ for $2 \leqslant n \leqslant 21$, corresponding to the patterns' evolutions displayed in Fig. 2. Note that (a)–(c) $\delta = 0$ and (d)–(f) $\delta = 1$. All physical parameters, initial conditions, and random phases are identical to those utilized in Fig. 2.

To characterize the impact of the capillary number on the morphologies of the nonlinear interfacial structures under the presence of viscous normal stresses for a range of values of Ca, we analyze Fig. 5. It details how the rescaled perimeter of the fluid-fluid interfaces at final time t_f,

$$L(t_f) = \frac{1}{2\pi R(t_f)} \int_0^{2\pi} \sqrt{\mathcal{R}^2(t_f) + \left[\frac{d\mathcal{R}(t_f)}{d\theta}\right]^2} \, d\theta, \quad (18)$$

behaves as Ca is increased. $L(t_f)$ expresses the ratio of the perimeter of the perturbed interface $\mathcal{R}(t)$ to the length of the corresponding unperturbed, circular interface of radius $R(t)$ at the final time $t = t_f$. $L(t_f)$ reflects the departure from a circle at the final time t_f, serving as a quantitative measure of the increase in complexity of the interface at nonlinear stages of the dynamics. The larger the rescaled perimeter $L(t_f)$, the more structured the interface. For each value of Ca, the data shown in Fig. 5 are obtained from the third-order time evolution of interfaces generated for modes $2 \leqslant n \leqslant 21$, by taking into account viscous normal stresses effects ($\delta = 1$), and produced by employing the same set of phases utilized in Fig. 2(f). In addition, $A = 1$. The rest of the parameters are also identical to those used in Fig. 2(f). Figure 5 considers 15 increasing values of the capillary number in the range $25 \leqslant \text{Ca} \leqslant 200$, separated by equal steps of $\text{Ca} = 12.5$. From Fig. 5 it is apparent that the rescaled interfacial perimeter increases for increasingly larger values of Ca, indicating that the third-order nonlinear interfaces become more deformed
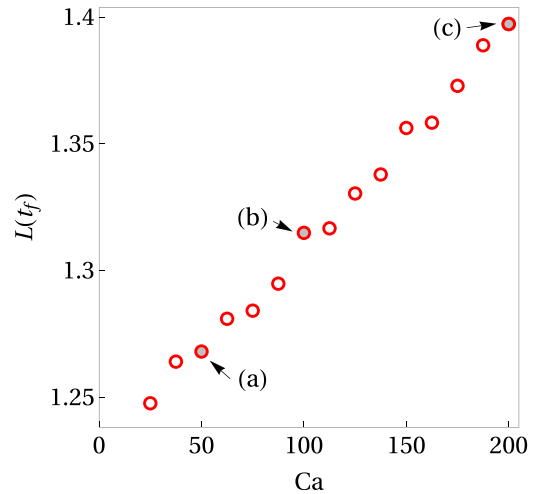

FIG. 5. Rescaled interfacial perimeters $L(t_f)$ [Eq. (18)] for third-order nonlinear patterns obtained by considering different values of the capillary number Ca. Here $A = 1$ and $\delta = 1$. The data are acquired by using the set of phases and the rest of the parameters utilized in Fig. 2(f). The weakly nonlinear, third-order time evolution of the interfacial shapes corresponding to points (a) Ca = 50, (b) Ca = 100, and (c) Ca = 200 (identified by small arrows) are presented in Fig. 6.
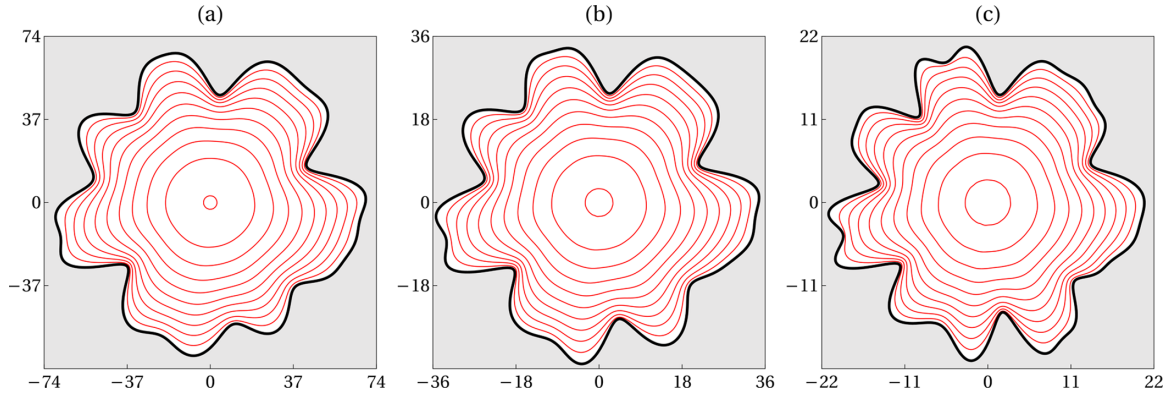
FIG. 6. Time evolution of the interfacial patterns associated with the data points (a)–(c) indicated in Fig. 5. The growth of these structures is generated by solving Eq. (13) for $2 \leqslant n \leqslant 21$, $0 \leqslant t \leqslant t_f$, equal time intervals $\Delta t = t_f/10$, $\delta = 1$, and considering that $A = 1$, for three increasing values of the capillary number: (a) Ca = 50, (b) Ca = 100, and (c) Ca = 200. These patterns are obtained by using the set of phases already utilized in Fig. 2(f). The values of t_f are (a) 12 000, (b) 3000, and (c) 1060.

as Ca is augmented. This will have consequences on the development of fingertip-tripling phenomena (see Fig. 6).

The effect of varying the capillary number on the emergence of fingertip-tripling events is inspected in Fig. 6. We carry out our analysis on this issue by illustrating the weakly nonlinear, third-order time evolution of the patterns that arise for the data points (a) Ca = 50, (b) Ca = 100, and (c) Ca = 200, indicated by arrows in Fig. 5. By scrutinizing Fig. 6, in particular the fingers located on the upper right side of the patterns in Figs. 6(a)–(c), one notices that by augmenting the value of the capillary number Ca the result is an enhanced tendency toward fingertip-tripling formation, in accordance with the expected increase in interface instability as revealed by Fig. 5. Although the formation of conventional tip splitting (or, tip doubling) is not the main focus of this work, one can also notice in Fig. 6 that this phenomenon is also enhanced as Ca assumes larger values (see, for instance, the finger on the upper left-hand side of the patterns). This is in line with previous findings in the literature [21].

As in all other situations analyzed in our study, in trying to capture the occurrence of tip-tripling events via our perturbative mode-coupling analysis, there is a tradeoff between the desire of using as large as possible destabilizing parameters (in order to detect sizable morphological effects), and the limitations imposed by a perturbative scheme (requirement of smallness of perturbations with respect to the unperturbed evolving interface radius, and necessity of avoiding unphysical interface crossings). This can be seen in Fig. 6, where tip tripling of the finger situated on the upper right-hand side of the patterns is only clearly unveiled in Fig. 6(c), for the largest Ca, and consequently, for the smallest final time t_f. Tip tripling is not detected in such a finger for smaller values Ca: in Fig. 6(a) one detects the onset of tip doubling, while in Fig. 6(b) a fingertip-flattening behavior is identified. From the weakly nonlinear findings of Figs. 5 and 6 which explored a range of values for the capillary number, one concludes that the occurrence of fingertip tripling is indeed favored for larger values of Ca. We point out that we have observed a similar morphological trend (i.e., enhanced tip tripling) as Ca is increased for other sets of random phases.

Nevertheless, we emphasize that, even though the use of higher Ca is a necessary condition to get fingertip tripling, this is not a sufficient condition. For example, recall that the pattern displayed in Fig. 2(c), which is produced by utilizing basically the very same parameter values and initial conditions as those utilized to obtain the structure illustrated in Fig. 6(c) [or in Fig. 2(f)], does not show the development fingertip tripling. It turns out that the only differing condition in the way the patterns shown in Figs. 2(c) and 6(c) are generated is the fact that while the former neglects the action of viscous normal stresses ($\delta = 0$), the latter takes it into account ($\delta = 1$). Therefore, to predict and capture fingertip tripling via theoretical means it is not enough just to consider higher values of the capillary number [e.g., Ca = 200, as in Figs. 2(c) and 6(c)], but on top of it one must take into account the action of viscous normal stresses.

We close our discussion by examining what happens to fingertip-tripling phenomena under the presence of normal stresses ($\delta = 1$), if the capillary number is held fixed, while the viscosity contrast is modified. This is done in Fig. 7 for Ca = 200, $2 \leqslant n \leqslant 21$, and $0 \leqslant t \leqslant t_f$. Here we consider the emerging interface shapes for three values of the viscosity contrast: (a) $A = 0.75$, (b) $A = 0.85$, and (c) $A = 1$. These patterns are generated by using the same set of phases applied in Fig. 2(f). Going over Fig. 7, and again paying closer attention to the fingers growing on the upper right-hand side of the images, one can verify that fingertip-tripling formation is favored when the viscosity contrast assumes larger values. Focusing precisely on the finger on the upper right-hand corner, (i) there is no sign of tip tripling in Fig. 7(a), (ii) just a modest onset of tip tripling can be detected in Fig. 7(b) (small bump arising in the middle of the finger), and (iii) only in Fig. 7(c) is a clear tip-tripling finger observed. Of course, if A is decreased further the interfacial patterns become increasingly more stable. As a matter of fact, the experimental cases that reveal some tip-tripling events in injection-driven radial Hele-Shaw flows [22] are all performed for large values of the viscosity contrast ($A = 1$). We have also investigated the behavior of the rescaled interfacial perimeter $L(t_f)$ for Ca = 200 as the viscosity contrast A varies in the range of values leading to unstable displacements (i.e., $0 < A \leqslant 1$),
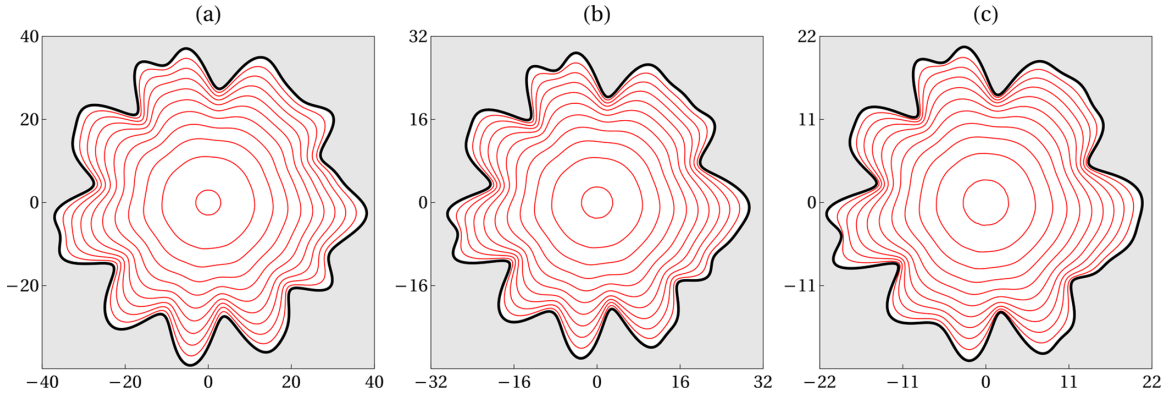
FIG. 7. Time evolution of the interfacial patterns generated by solving Eq. (13) for $2 \leqslant n \leqslant 21$, $0 \leqslant t \leqslant t_f$, equal time intervals $\Delta t = t_f/10$, $\delta = 1$, and considering Ca = 200, for three increasing values of the viscosity contrast: (a) $A = 0.75$, (b) $A = 0.85$, and (c) $A = 1$. These patterns are generated by using the set of phases utilized in Fig. 2(f). The values of t_f are (a) 2700, (b) 1550, and (c) 1060.

and, similar to what we have found in Fig. 5, we encountered that $L(t_f)$ increases with A. Note that the behaviors of the interfaces in Fig. 7 are consistent with this fact, once deformed interfaces are obtained earlier in time (smaller t_f) for larger values of A, in consonance with the well known, typical behavior of the Saffman-Taylor instability in Hele-Shaw flows [1]. Notice that we have checked that an increased tendency toward tip-tripling formation also occurs for $A = 1$, if other sets of random phases are used.

At this moment, we do not have a fully quantitative, definite physical mechanism by which such fingertip-tripling structures are formed. Nonetheless, on the basis of the main findings of this work, we would like to conclude by offering some qualitative physical elements that could contribute to their formation. For the case of conventional fingertip splitting via tip doubling, it is well known that the critical length scale leading to fingertip bifurcation increases at higher capillary numbers Ca [1,23]. We believe a similar physical mechanism acts to generate fingertip tripling. If Ca and A are sufficiently large, and in addition viscous normal stresses effects are such that local velocities increase, the growing fingers would be more susceptible to the viscous fingering instability. In this process the evolving fingers tend to widen, making room to further destabilization. This means that it would be easier for more fingers to form at the expanding tips, ultimately favoring the occurrence of fingertip-tripling events. We hope our current investigation will stimulate researchers to find a better and more quantitative physical explanation for the rising of these interesting three-fingered shapes.

It should be stressed that, as unveiled in Refs. [2–7], experiments reveal the simultaneous occurrence of both tip doubling and tip tripling. Therefore, as pointed out above, if Ca and A are sufficiently large, both tip doubling and tip tripling are favored. Other than these, there are no specific configurations or physical constraints required to lead to tip tripling experimentally. Nevertheless, it is the inclusion of the effects of viscous normal stresses into the theoretical perturbative description of the problem that allows one to capture the development of the tip-tripling phenomena detected experimentally. In other words, if viscous normal stresses are neglected in the modified Young-Laplace condition [Eq. (7)], our theory is able to reproduce tip-doubling events, but not tip tripling. On the other

hand, the inclusion of viscous normal stresses in Eq. (7) are such that local velocities increase, resulting in the rising of tip-doubling and tip-tripling fingered structures at third order.

IV. CONCLUDING REMARKS

In this work, we carried out a perturbative mode-coupling analysis of the radial viscous fingering problem in Hele-Shaw geometry, and derived nonlinear, coupled differential equations that describe the time evolution of the interfacial perturbation amplitudes accurate to third order. As opposed to most previous theoretical studies of the viscous fingering instability, our model incorporates the effects of viscous normal stresses on the dynamical evolution of interfacial pattern-forming structures. In addition to the customary development of fingertip doubling, our model predicts the occurrence of fingertip-tripling events, where a finger splits into three others. Our findings suggest that normal viscous stresses are an important physical ingredient leading to the formation of fingertip tripling in radial Hele-Shaw flows induced by injection.

Our theoretical results are in qualitative agreement with existing experimental observations, where the emergence of fingertip tripling has been identified [2–7,22]. These results indicate that viscous normal stresses exert a dual role on the time evolution of the interface. They tend to restrain the overall growth and delay the formation of interfacial disturbances. However, they also modify the speed of propagation of the interface, and alter the local interfacial velocity distribution in such a way that fingers may split into two, as well as into three secondary fingers. We have verified that the manifestation of the tip-tripling phenomena via our perturbative model is robust, persisting to occur under the presence of background noise, under different initial conditions, and for a range of possible values for the capillary number Ca, and viscosity contrast A. We have also found that fingertip-tripling episodes are facilitated for larger values of Ca and A.

Unfortunately, due to the intrinsic limitations of our perturbative model, which is valid only at the onset of nonlinear effects, we have not been able to perform a quantitative and direct comparison between our weakly nonlinear patterns exhibiting tip tripling and the corresponding three-fingered structures detected experimentally. These particular

experiments [2–7,22] usually reveal tip-tripling events at advanced time, fully nonlinear stages of the dynamics for which the interface is highly deformed. Regrettably, our perturbative theory no longer holds under these conditions. Despite the possible nontrivial challenges related to the inclusion of viscous normal stresses effects in a numerical scheme capable of accurately describing the long time dynamics of the system, the development of fully nonlinear numerical simulations for the problem is a possible extension of this work. We plan to tackle these significantly more complex issues in a future work.

APPENDIX A: DERIVATION OF THE MODIFIED PRESSURE DIFFERENCE BOUNDARY CONDITION EQ. (7)

In this Appendix, we derive the generalized pressure jump boundary condition [Eq. (7)], by incorporating contributions from viscous normal stresses and surface tension. We follow Refs. [9,29–31], and consider the normal stress balance at the interface ($r = \mathcal{R}$) of two viscous Newtonian, incompressible fluids ($j = 1$ and 2) in which stresses are related to pressures and velocities as

$$p_1 - p_2 = \sigma\kappa + [\delta(\tau_1 - \tau_2) \cdot \mathbf{n}] \cdot \mathbf{n}, \tag{A1}$$

where

$$\tau_j = \eta_j[\boldsymbol{\nabla}\mathbf{v}_j + (\boldsymbol{\nabla}\mathbf{v}_j)^T], \tag{A2}$$

with T denoting a matrix transpose, and $\delta = 1$ ($\delta = 0$) if normal stresses are (not) taken into account. In the effectively two-dimensional flow geometry of a radial Hele-Shaw cell, the stress tensor is represented in polar coordinates (r, θ) as

$$\tau_j = \begin{pmatrix} \tau_{j,rr} & \tau_{j,r\theta} \\ \tau_{j,r\theta} & \tau_{j,\theta\theta} \end{pmatrix}. \tag{A3}$$

By considering the incompressibility of the fluids [Eq. (4)], the components of the stress tensor are given by

$$\tau_{j,rr} = 2\eta_j\left[\frac{\partial v_{j,r}}{\partial r}\right], \tag{A4}$$

$$\tau_{j,\theta\theta} = 2\eta_j\left[\left(\frac{1}{r}\frac{\partial v_{j,\theta}}{\partial \theta} + \frac{v_{j,r}}{r}\right)\right], \tag{A5}$$

$$\tau_{j,r\theta} = \eta_j\left[r\frac{\partial}{\partial r}\left(\frac{v_{j,\theta}}{r}\right) + \frac{1}{r}\frac{\partial v_{j,r}}{\partial \theta}\right]. \tag{A6}$$

These components can be conveniently expressed in terms of the velocity potentials ϕ_j, yielding

$$\tau_{j,rr} = -2\eta_j\left[\frac{\partial^2 \phi_j}{\partial r^2}\right], \tag{A7}$$

$$\tau_{j,\theta\theta} = -2\eta_j\left[\frac{1}{r^2}\frac{\partial^2 \phi_j}{\partial \theta^2} + \frac{1}{r}\frac{\partial \phi_j}{\partial r}\right], \tag{A8}$$

$$\tau_{j,r\theta} = 2\eta_j\left[\frac{1}{r^2}\frac{\partial \phi_j}{\partial \theta} - \frac{1}{r}\frac{\partial^2 \phi_j}{\partial r\partial \theta}\right]. \tag{A9}$$

With Eqs. (A7)–(A9) at hand, and with the unit normal vector written as $\mathbf{n} = (n_r, n_\theta)$, one can readily see that

$$\begin{aligned} [\tau_j \cdot \mathbf{n}] \cdot \mathbf{n} &= \left[\begin{pmatrix} \tau_{j,rr} & \tau_{j,r\theta} \\ \tau_{j,r\theta} & \tau_{j,\theta\theta} \end{pmatrix}\begin{pmatrix} n_r \\ n_\theta \end{pmatrix}\right]^T\begin{pmatrix} n_r \\ n_\theta \end{pmatrix} \\ &= n_r^2\tau_{j,rr} + 2n_r n_\theta\tau_{j,r\theta} + n_\theta^2\tau_{j,\theta\theta} \\ &= -2\eta_j\left[n_r^2\frac{\partial^2 \phi_j}{\partial r^2} + 2n_r n_\theta\left(\frac{1}{r}\frac{\partial^2 \phi_j}{\partial r\partial \theta} - \frac{1}{r^2}\frac{\partial \phi_j}{\partial \theta}\right)\right. \\ &\quad \left. + n_\theta^2\left(\frac{1}{r^2}\frac{\partial^2 \phi_j}{\partial \theta^2} + \frac{1}{r}\frac{\partial \phi_i}{\partial r}\right)\right]. \end{aligned} \tag{A10}$$

Finally, by evaluating Eq. (A10) for fluids $j = 1$ and 2, and substituting the resulting expressions into Eq. (A1), ones gets Eq. (7).

APPENDIX B: EXPRESSIONS FOR THE NONLINEAR MODE-COUPLING FUNCTIONS

This Appendix presents the expressions of the nonlinear mode-coupling functions F, S_F, G, S_G, H, S_H, I, S_I, J, S_J, K, and S_K presented in Eq. (9):

$$F(n, p) = \frac{|n|}{s(n)R}\left\{\frac{1}{2\pi R^2}A\left(\frac{1}{2} - \text{sgn}(np)\right) - \frac{(A+1)}{2\text{Ca}R^3}\left(1 - \frac{1}{2}p(n+3p)\right)\right\}, \tag{B1}$$

$$S_F(n, p) = \delta\frac{|n|}{12\pi R^5 s(n)}\{-A[n|n|\text{sgn}(p) - p^2 + 1] + |p| + n\text{sgn}(p)\}, \tag{B2}$$

$$G(n, p) = \frac{1}{s(n)R}\{A|n|[1 - \text{sgn}(np)] - 1\}, \tag{B3}$$

$$S_G(n, p) = \delta\frac{|n|}{6R^3 s(n)}\{-A[n|n|\text{sgn}(p) - 2np + p^2 - 1] - |n| + |p| + n\text{sgn}(p)\}, \tag{B4}$$

$$H(n, p, q) = \frac{|n|q}{2\pi s(n)R^4}\text{sgn}(p)\left[1 - \text{sgn}(nq) - \frac{A}{|n|}\right], \tag{B5}$$

$$S_H(n, p, q) = -\delta\frac{|n|}{12\pi R^6 s(n)}\{\text{sgn}(npq)[(q^2 - 1)|q|\text{sgn}(n) - 2q|nq| + n^2 q] - A\,\text{sgn}(pq)[q(n+q) - |nq|]\}, \tag{B6}$$

$$I(n, p, q) = \frac{1}{s(n)R^2}\left\{A|n|[1 - \text{sgn}(nq)] + |n||q|\,\text{sgn}(pq)\left[1 - \text{sgn}(nq) - \frac{A}{|n|}\right] - 1\right\}, \tag{B7}$$

$$S_I(n, p, q) = -\delta\frac{|n|}{3R^4 s(n)}(\{q\text{sgn}(p)[n|n|\text{sgn}(q) - 2nq + q^2 - 1] + |n| - (n + q)\text{sgn}(q)\}$$

$$- A\{|q|(n + q)\text{sgn}(p) - |n|[n\text{sgn}(q) + q\text{sgn}(p)] + 2nq - q^2 + 1\}), \tag{B8}$$

$$J(n, p, q) = \frac{1}{2\pi s(n)R^4}\left\{\frac{(A - 1)\mathcal{A}(n, p, q) + (A + 1)\mathcal{B}(n, p, q)}{2|p|} - \frac{|n|(|p| + A/3)}{2} - 1\right\}$$

$$+ \frac{(A + 1)|n|}{2\text{Ca}R^5}\left\{1 - 3p^2 - \frac{3}{2}q(n - p - q)(p^2 + 1)\right\}, \tag{B9}$$

$$S_J(n, p, q) = -\delta\frac{|n|}{24\pi R^6 s(n)}\{A[4|n|(q - n)\text{sgn}(p) + |np| - 2n(p + 2q) + 7p^2 + 18pq + 4q^2 - 2]$$

$$+ p|n|(-2n + p + 2q) + \text{sgn}(p)[4q(np + 3) - 4n + p^3 - 4pq^2 - 3\text{sgn}(p) + 12p] + 3\}, \tag{B10}$$

$$K(n, p, q) = \frac{1}{s(n)R^2}\left\{\frac{(A - 1)\mathcal{A}(n, p, q) + (A + 1)\mathcal{B}(n, p, q)}{2|p|} - \frac{|n|(|p| + A)}{2}\right\}, \tag{B11}$$

$$S_K(n, p, q) = \delta\frac{|n|}{12R^4 s(n)}(- A[|n|\text{sgn}(p)(-4n + p + 4q) - 2np + 4nq + 7p^2 + 10pq - 4q^2 + 4]$$

$$+ |n|\{-[p(-2n + p + 2q) - 2]\} - \text{sgn}(p)[4q(np + 3) - 4n + p^3 - 4pq^2 + 12p]), \tag{B12}$$

where the auxiliary functions $\mathcal{A}(n, p, q)$ and $\mathcal{B}(n, p, q)$ are expressed as

$$\mathcal{A}(n, p, q) = (n - p - q)(2p - p|p|) - \frac{1}{2}|p|(|p| - 1)(|p| - 2), \tag{B13}$$

and

$$\mathcal{B}(n, p, q) = (n - p - q)(2p + p|p|) + \frac{1}{2}|p|(|p| + 1)(|p| + 2). \tag{B14}$$

Note that the sgn function equals ± 1 according to the sign of its argument.

[1] For review papers see, for example, G. M. Homsy, Viscous fingering in porous media, Annu. Rev. Fluid Mech. **19**, 271 (1987); K. V. McCloud and J. V. Maher, Experimental perturbations to Saffman-Taylor flow, Phys. Rep. **260**, 139 (1995); J. Casademunt, Viscous fingering as a paradigm of interfacial pattern formation: Recent results and new challenges, Chaos **14**, 809 (2004).

[2] L. Paterson, Radial fingering in a Hele-Shaw cell, J. Fluid Mech. **113**, 513 (1981).

[3] J. D. Chen, Radial viscous fingering patterns in Hele-Shaw cells, Exp. Fluids **5**, 363 (1987).

[4] J. D. Chen, Growth of radial viscous fingers in a Hele-Shaw cell, J. Fluid Mech. **201**, 223 (1989).

[5] E. Lajeunesse and Y. Couder, On tip splitting instability of viscous fingers, J. Fluid Mech. **419**, 125 (2000).

[6] T. Ward and A. R. White, Gas-driven displacement of a liquid in a partially filled radial Hele-Shaw cell, Phys. Rev. E **83**, 046316 (2011).

[7] D. Pihler-Puzović, G. G. Peng, J. R. Lister, M. Heil, and A. Juel, Viscous fingering in a radial elastic walled Hele-Shaw cell, J. Fluid Mech. **849**, 163 (2018).

[8] P. G. Saffman and G. I. Taylor, The penetration of a fluid into a porous medium or Hele-Shaw cell containing a more viscous liquid, Proc. R. Soc. London, Ser. A **245**, 312 (1958).

[9] L. D. Landau and E. M. Lifshitz, *Course of Theoretical Mechanics: Fluid Mechanics* (Pergamon, New York, 1959), Vol. 6.

[10] E. Alvarez-Lacalle, J. Ortín, and J. Casademunt, Low viscosity contrast fingering in a rotating Hele-Shaw cell, Phys. Fluids **16**, 908 (2004).

[11] H. Kim, T. Funada, D. D. Joseph, and G. M. Homsy, Viscous potential flow analysis of radial fingering in a Hele-Shaw cell, Phys. Fluids **21**, 074106 (2009).

[12] M. K. Awasthi, R. Asthana, and G. S. Agrawal, Pressure corrections for viscous potential flow analysis of radial fingering in Hele-Shaw cell, J. Eng. Math. **83**, 131 (2013).

[13] M. Nagel and F. Gallaire, A new prediction of wavelength selection in radial viscous fingering involving normal and tangential stresses, Phys. Fluids **25**, 124107 (2013).

[14] P. H. A. Anjos, E. O. Dias, L. Dias, and J. A. Miranda, Adhesion force in fluids: Effects of fingering, wetting, and viscous normal stresses, Phys. Rev. E **91**, 013003 (2015).

[15] L. N. Brush, R. F. Sekerka, and G. B. McFadden, A numerical and analytical study of nonlinear bifurcations associated with the morphological stability of two-dimensional single crystals, J. Cryst. Growth **100**, 89 (1990).

[16] S. W. Haan, Weakly nonlinear hydrodynamic instabilities in inertial fusion, Phys. Fluids B **3**, 2349 (1991).

[17] J. A. Miranda and M. Widom, Radial fingering in a Hele-Shaw cell: A weakly nonlinear analysis, Phys. D (Amsterdam, Neth.) **120**, 315 (1998).

[18] E. Alvarez-Lacalle, E. Pauné, J. Casademunt, and J. Ortín, Systematic weakly nonlinear analysis of radial viscous fingering, Phys. Rev. E **68**, 026308 (2003).

[19] P. H. A. Anjos and S. Li, Weakly nonlinear analysis of the Saffman-Taylor problem in a radially spreading fluid annulus, Phys. Rev. Fluids **5**, 054002 (2020).

[20] H. Gadêlha and J. A. Miranda, Finger competition dynamics in rotating Hele-Shaw cells, Phys. Rev. E **70**, 066308 (2004).

[21] H. Gadêlha and J. A. Miranda, Effects of normal viscous stresses on radial viscous fingering, Phys. Rev. E **79**, 066312 (2009).

[22] Illustrative examples for the occurrence of fingertip tripling in injection-driven radial Hele-Shaw flow experiments can be found in Fig. 1 in [2], Fig. 3(a) in [3], Fig. 1(c) in [4], Fig. 17(b) in [5], Fig. 2 in [6], and Fig. 1(d) in [7].

[23] S. J. Jackson, D. Stevens, D. Giddings, and H. Power, Dynamic-wetting effects in finite-mobility-ratio Hele-Shaw flow, Phys. Rev. E **92**, 023021 (2015).

[24] J. R. Dormand and P. J. Prince, A family of embedded Runge-Kutta formulae, J. Comp. Appl. Math. **6**, 19 (1980).

[25] L. F. Shampine and M. W. Reichelt, The MATLAB ODE Suite, SIAM J. Sci. Comput. **18**, 1 (1997).

[26] M. J. P. Gingras and Z. Rácz, Noise and the linear stability analysis of viscous fingering, Phys. Rev. A **40**, 5960 (1989).

[27] E. O. Dias and J. A. Miranda, Wavelength selection in Hele-Shaw flows: A maximum-amplitude criterion, Phys. Rev. E **88**, 013016 (2013).

[28] S. S. S. Cardoso and A. W. Woods, The formation of drops through viscous instability, J. Fluid Mech. **289**, 351 (1995).

[29] R. L. Panton, *Incompressible Flow* (Wiley, Hoboken, 2013).

[30] G. K. Batchelor, *An Introduction to Fluid Dynamics* (Cambridge University Press, Cambridge, UK, 1967).

[31] W. E. Langlois and M. O. Deville, *Slow Viscous Flow*, 2nd ed. (Springer, New York, 2014).